

# Scaling behavior of thermal conductivity in single-crystalline $\alpha$ -Fe<sub>2</sub>O<sub>3</sub> nanowires\*

Qilang Wang(王啟浪)<sup>1,†</sup>, Yuyu Chen(陈允玉)<sup>2,†</sup>, Adili Aiyiti(阿地力·艾依提)<sup>1,†</sup>, Minrui Zheng(郑敏锐)<sup>3</sup>, Nianbei Li(李念北)<sup>4,‡</sup>, and Xiangfan Xu(徐象繁)<sup>1,§</sup>

<sup>1</sup>Center for Phononics and Thermal Energy Science, China-EU Joint Center for Nanophononics, School of Physics Science and Engineering, Tongji University, Shanghai 200092, China

<sup>2</sup>The First Affiliated Hospital of Wenzhou Medical University, Wenzhou 325000, China

<sup>3</sup>Department of Electrical and Computer Engineering, Faculty of Engineering, National University of Singapore, 4 Engineering Drive 3, Singapore 117583

<sup>4</sup>Institute of Systems Science and Department of Physics, College of Information Science and Engineering, Huaqiao University, Xiamen 361021, China

(Received 25 March 2020; revised manuscript received 30 April 2020; accepted manuscript online 7 May 2020)

Unveiling the thermal transport properties of various one-dimensional (1D) or quasi-1D materials like nanowires, nanotubes, and nanorods is of great importance both theoretically and experimentally. The dimension or size dependence of thermal conductivity is crucial in understanding the phonon–phonon interaction in the low-dimensional systems. In this paper, we experimentally investigate the size-dependent thermal conductivity of individual single crystalline  $\alpha$ -Fe<sub>2</sub>O<sub>3</sub> nanowires collaborating the suspended thermal bridge method and the focused electron-beam self-heating technique, with the sample diameter ( $d$ ) ranging from 180 nm to 661 nm and length ( $L$ ) changing from 4.84  $\mu$ m to 20.73  $\mu$ m. An empirical relationship for diameter-/length-dependent thermal conductivity is obtained, which shows an approximately linear dependence on the aspect ratio ( $L/(1 + Cd)$ ) at  $T = 300$  K, where  $C$  is a fitting parameter. This is related to the boundary scattering and diameter effect of  $\alpha$ -Fe<sub>2</sub>O<sub>3</sub> nanowires although rigorous calculations are needed to confirm the result.

**Keywords:** thermal conductivity, size-dependent, boundary scattering, nanowire

**PACS:** 44.10.+i, 63.22.–m, 63.20.–e

**DOI:** 10.1088/1674-1056/ab90f0

## 1. Introduction

On Mars, the existence of hematite ( $\alpha$ -Fe<sub>2</sub>O<sub>3</sub>) was confirmed by the Curiosity Rover, which is partly responsible for the red tone, and its analysis provides valuable clues to the history of liquid water in the planet's environment.<sup>[1]</sup> Here on Earth, iron is one of the most abundant elements while iron oxides are ubiquitous in nature, among which hematite is the most common morphology due to its high thermodynamic stability.<sup>[2]</sup> Iron oxides are inexpensive, environment-friendly, and corrosion-resistant materials that have various novel applications in many aspects, e.g., catalysts/photocatalysts,<sup>[3–5]</sup> gas sensing,<sup>[6,7]</sup> drug delivery,<sup>[8]</sup> gene therapy,<sup>[9]</sup> photoelectrochemical water splitting,<sup>[10]</sup> and energy storage.<sup>[11]</sup> Hence, scientists including biologists, chemists, physicists, geologists, and engineers have all displayed the liveliest interests in iron oxides.

In recent years, various one-dimensional (1D) or quasi-1D materials like nanowires, nanotubes, and nanorods have attracted wide interests, due to the exotic dimensional/size dependent properties which are different from their bulk

counterparts and have potential applications in miniaturized electronic and energy conversion devices.<sup>[12–21]</sup> As the peculiar properties and applications of  $\alpha$ -Fe<sub>2</sub>O<sub>3</sub> are closely related to the dimension, shape, and surface morphology, amount of researches were focused on relevant investigations, e.g., synthesis and characterization of  $\alpha$ -Fe<sub>2</sub>O<sub>3</sub> nanoparticles, nanorod, and nanowires by controlling the experimental conditions and parameters in various methods.<sup>[22–27]</sup> In particular, synthesis<sup>[22]</sup> of  $\alpha$ -Fe<sub>2</sub>O<sub>3</sub> nanowires has attracted much attention and some of the intrinsic physical properties including electrical,<sup>[23]</sup> optical,<sup>[24]</sup> and magnetic<sup>[25–27]</sup> properties were investigated. However, one of the most basic and important properties of  $\alpha$ -Fe<sub>2</sub>O<sub>3</sub> nanowires, the thermal conductivity, is still missing as far as we know.

Here, we synthesized  $\alpha$ -Fe<sub>2</sub>O<sub>3</sub> nanowire arrays vertically on the surface of the substrate by oxidation of pure iron. We demonstrated the size-dependent thermal conductivity of individual single crystalline  $\alpha$ -Fe<sub>2</sub>O<sub>3</sub> nanowires with the thermal bridge method and focused electron beam self-heating technique.

\*Project supported by the Key-Area Research and Development Program of Guangdong Province, China (Grant No. 2020B010190004), the National Natural Science Foundation of China (Grant Nos. 11674245, 11775158, 11890703, and 11935010), and the Open Fund of Zhejiang Provincial Key Laboratory of Quantum Technology and Device, China (Grant No. 20190301), and the Shanghai Committee of Science and Technology in China (Grant Nos. 17142202100, 17ZR1447900, and 17ZR1432600).

†These authors contributed equally to this work.

‡Corresponding author. E-mail: nbli@hqu.edu.cn

§Corresponding author. E-mail: xuxiangfan@tongji.edu.cn

© 2020 Chinese Physical Society and IOP Publishing Ltd

<http://iopscience.iop.org/cpb> <http://cpb.iphy.ac.cn>

## 2. Experimental methods and sample characterization

**Synthesis** A high purity of iron foil, ultrasonically cleaned with ethanol, was used to synthesize the nanowires both as reagent and substrate. The foil with some metal catalyst carried by the quartz boat was placed in the quartz tube reactor, which was heated to 800 °C in the Ar gas environment with the flow rate of 500 standard cubic centimeter per minute (sccm). An oxygen flow with the rate of 30 sccm was introduced for reaction for 0.5–1 h. With Ar gas keeping flowing, the tube was cooled down to room temperature.

**Morphology characterization** The morphology and crystal structure of the as-grown nanowires were characterized by scanning electron microscopy (FEI SEM Nova 450), transmission electron microscopy (TEM JEOL JEM-2100 F), x-ray diffraction (XRD D8), and Raman spectroscopy (HR800). Figure 1(a) shows the TEM image of the individual  $\alpha$ -Fe<sub>2</sub>O<sub>3</sub> nanowire. The HRTEM image (Fig. 1(b)) and FFT ED pattern (inset) reveal the single-crystalline rhombohedral structure and preferred growth direction [110], which is further confirmed by the XRD pattern (Fig. 1(c)), showing the extensive intensity peak corresponding to the [110] direction. The room temperature Raman spectrum (Fig. 1(d)) shows strong Raman resonant peaks at 225 cm<sup>-1</sup>, 244 cm<sup>-1</sup>, 295 cm<sup>-1</sup>, 410 cm<sup>-1</sup>, 501 cm<sup>-1</sup>, and 609 cm<sup>-1</sup> with tiny frequency shift, which may originate from the higher crystalline arrangement of the  $\alpha$ -Fe<sub>2</sub>O<sub>3</sub> nanowires.

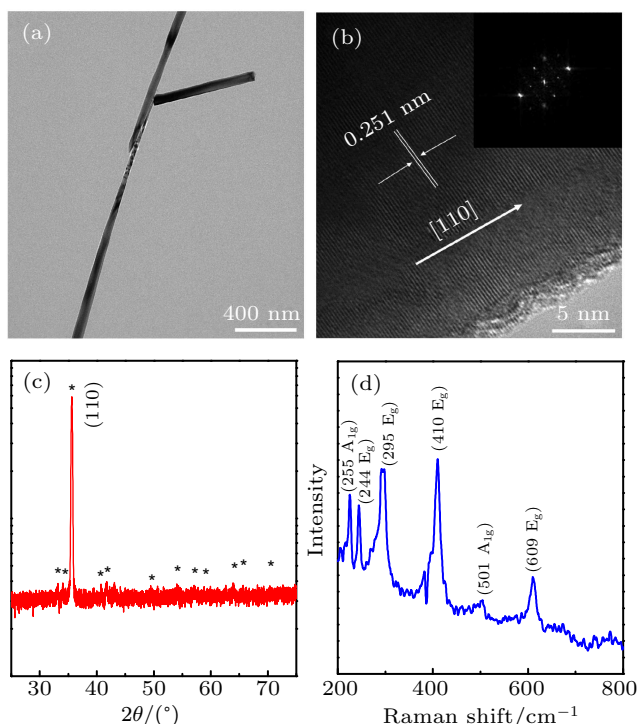


**Fig. 1.** Sample characterization. (a) TEM image of the single  $\alpha$ -Fe<sub>2</sub>O<sub>3</sub> nanowire. (b) HRTEM image and FFT ED pattern revealing single crystal structure of the nanowire. (c) XRD patterns and (d) Raman spectrum of the  $\alpha$ -Fe<sub>2</sub>O<sub>3</sub> nanowires.

**Suspended sample preparation** The suspended microdevices applied for thermal measurements were fabricated with the similar standard lithography, metal deposition/lift-off technique, deep RIE, and wet etching process as shown in the reference.<sup>[28–32]</sup> The as-prepared null devices were annealed at 250 °C in H<sub>2</sub>/Ar atmosphere for 2–3 hours, with which the possible residues on the surface of the devices were cleaned. Since the grass-like grown nanowires rooted to the substrate (Fig. 2(a)), it is difficult to separate individual nanowires. Hence, we transferred some free lying nanowires on the silicon substrate (Fig. 2(b)). The micromanipulator miBot<sup>TM</sup> armed with a sharp tungsten tip (Fig. 2(c)) was used to manipulate and transfer the individual nanowires on the as-prepared suspended devices (Fig. 2(d)). Electron beam induced Pt/C deposition (EBID) process was carried out to fix the two ends of the nanowires on the devices, by which the contacts were enhanced.<sup>[33,34]</sup>

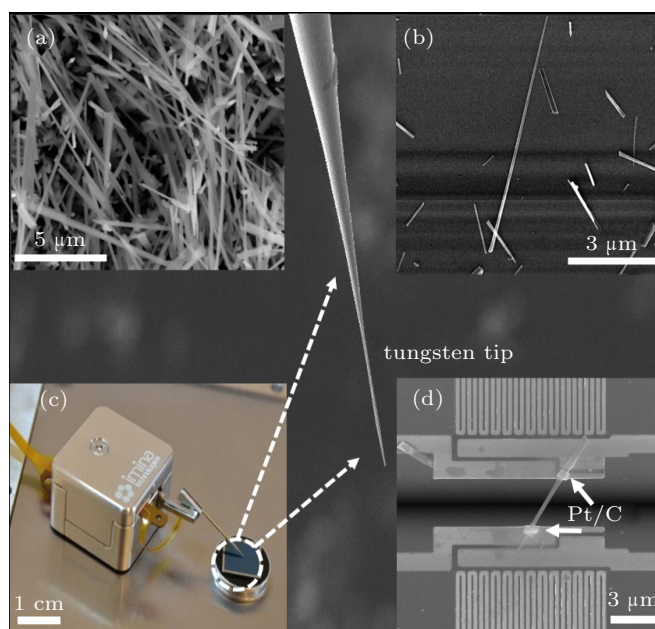


**Fig. 2.** Suspended sample preparation. (a) SEM image of the grass-like grown  $\alpha$ -Fe<sub>2</sub>O<sub>3</sub> nanowire arrays on the Fe foil. (b) SEM image of some free lying individual  $\alpha$ -Fe<sub>2</sub>O<sub>3</sub> nanowires on the SiO<sub>2</sub>/Si substrate. (c) Image of the micromanipulator miBot<sup>TM</sup> armed with a sharp tungsten tip. (d) SEM image of the as-prepared suspended  $\alpha$ -Fe<sub>2</sub>O<sub>3</sub> nanowire whose two ends are fastened to the electrodes of the microdevice by EBID.

**Thermal conductivity measurements** Two approaches, the thermal bridge method<sup>[30–32,35]</sup> and the focused electron-beam self-heating technique,<sup>[36–38]</sup> were utilized to measure the thermal conductance and derive the thermal contact resistance of the samples, both based on the prepatterned suspended device. For the thermal bridge method, one membrane of the device acts as a heater, which is heated by a DC current, and the other acts as a sensor. The thermal conductance of the supporting Pt/SiN<sub>x</sub> beams and the sample can be written as

$$G_b = \frac{Q_{\text{tot}}}{\Delta T_h + \Delta T_s}, \quad (1)$$

$$G = \frac{G_b \Delta T_s}{\Delta T_h - \Delta T_s}, \quad (2)$$

where  $Q_{\text{tot}}$  is the total heat flow into the heater,  $\Delta T_h$  and  $\Delta T_s$  are the temperature rise in the heater and sensor, respectively. The thermal conductivity of the samples can be calculated as

$$\kappa = G \frac{L}{A}, \quad (3)$$

where  $L$  and  $A$  are the length and cross section area of the nanowires. For the focused electron-beam self-heating technique, the focused electron beam of SEM acts as a local heating spot scanning along the nanowire and both membranes act as the sensor. The cumulative thermal resistance ( $R_i(x)$ ) from the left membrane to the local heating spot is calculated as

$$R_i(x) = R_b \left[ \frac{\alpha_0 - \alpha_i(x)}{1 + \alpha_i(x)} \right], \quad (4)$$

$$\alpha_0 = \frac{\Delta T_{L0}}{\Delta T_{R0}}, \quad (5)$$

$$\alpha_i = \frac{\Delta T_L}{\Delta T_R}, \quad (6)$$

where  $R_b$  is the equivalent thermal resistance of the supporting beams connecting the left (or the right) membrane to the environment.  $\Delta T_{L0}$  and  $\Delta T_{R0}$  are the temperature rise of the left and right membranes measured with the thermal bridge method, respectively, while  $\Delta T_L$  and  $\Delta T_R$  are the corresponding temperature rise when scanning along the nanowire with the focused electron beam. The intrinsic thermal conductivity of the samples is calculated as

$$\kappa = \frac{1}{(dR_i/dx) \cdot A}, \quad (7)$$

where  $A$  is the cross-section area of the individual nanowire.

The focused electron-beam self-heating method was used to measure the intrinsic thermal resistance  $R_i$ . The total thermal resistance  $R$  was measured by the thermal bridge method. The thermal contact resistance  $R_c$  could be obtained by subtracting the intrinsic thermal resistance from the total thermal resistance, i.e.,  $R_c = R - R_i$ .

### 3. Results and discussion

In order to figure out the influence of the EBID process on the thermal contact resistance, the effect of contacts and the EBID process on the measured total thermal resistance and thermal contact resistance is discussed first. The lengths and diameters of the individual nanowires were measured with SEM after the EBID process. Dimensions of the measured samples are given in Table 1. Figure 3(a) shows the schematic of the typical EBID process. The gas injection system (GIS) of the SEM injects  $C_9H_6Pt$  (Pt/C) with a fixed rate of gas flow while the high energy focused electron beam continuously scans in the sleeted contact area of the nanowire and device. By controlling the injection time,

different thickness of Pt/C pad could be deposited. The relation between pad thickness  $H$  and deposition time is shown in Fig. 3(b). The deposition thickness/time depends on the diameter of the nanowire and the deposited pad is thick enough to cover the diameter of the nanowire, i.e.,  $H \geq d$ . As shown in Fig. 3(c), the intrinsic thermal conductivity of the nanowires could be obtained from the typical cumulative thermal resistance curve, which was measured with the electron-beam self-heating technique as shown in the schematic inset, by substituting the slope  $dR_i/dx$  of the curve in Fig. 3(c) using Eq. (7). The effect of the Pt/C pad thickness on the thermal conductance and conductivity of the individual nanowire was monitored with the thermal bridge method by measuring the thermal conductance of the individual nanowire after different time or different thickness Pt/C deposition. As shown in Fig. 3(d), the thermal conductance of sample 7 in Table 1 increased from  $\sim 6.5 \times 10^{-8} \text{ W}\cdot\text{K}^{-1}$  to  $\sim 8.1 \times 10^{-8} \text{ W}\cdot\text{K}^{-1}$  due to the reduction of the thermal contact resistance. The total thermal resistance of the specific nanowire decreased from  $\sim 1.6 \times 10^7 \text{ K}\cdot\text{W}^{-1}$  to  $\sim 1.2 \times 10^7 \text{ K}\cdot\text{W}^{-1}$  while the thermal contact resistance decreased from  $\sim 5.1 \times 10^6 \text{ K}\cdot\text{W}^{-1}$  to  $\sim 2.5 \times 10^6 \text{ K}\cdot\text{W}^{-1}$  (Fig. 3(e)). More intuitively, the ratio of thermal contact resistance was reduced from  $\sim 38\%$  to  $\sim 28\%$  for the first 5 min/100 nm and to  $\sim 20\%$  or less after the Pt/C pad was thick enough to cover the nanowire (Fig. 3(f)).

Figure 4(a) shows the measured thermal conductance  $G$  (Eq. (2)) for individual single-crystalline  $\alpha\text{-Fe}_2\text{O}_3$  nanowires of different sizes in the temperature range from 20 K to 300 K using the thermal bridge method. The thermal conductances increase monotonously and reach the peak values around  $T = 120\text{--}150 \text{ K}$ . The peak values shift toward lower temperature with the increasing  $L$ , which suggests that diameter scattering is dominant until  $T = 120 \text{ K}$  before Umklapp scattering dominates over the diameter scattering and further reduces the thermal conductance with the increasing temperature ( $T > 150 \text{ K}$ ). In the lower temperature range ( $T \leq 50 \text{ K}$ ), thermal conductance data for the thick nanowires follow  $\sim T^n$  ( $2 < n < 3$ ), which suggests that diameter scattering, independent of temperature and frequency, is the dominant factor. The thermal conductivities deviate slowly from  $T^3$  with the decreasing  $d$ , which may originate from changes in phonon dispersion due to the phonon confinement, since thermal conductivity follows  $\sim T$  in the one-dimensional limit. Also the phonon confinement effect would lead to reduction of group velocities,<sup>[39]</sup> which could be responsible for the deviation. However, the exact selection rule as well as the phonon-phonon scattering rate might be related to the specific phonon dispersion in the nanostructures.<sup>[40]</sup> Thus, more experiments should be carried out before a precise and rigorous explanation is given. In the higher temperature range ( $T \geq 200 \text{ K}$ ), the thermal conductance decreases rapidly with temperature as  $T^{-\alpha}$  (the exponent  $\alpha$  is in the range of 0.5–1), which is contrast to the temperature dependence observed for Si nanowires.<sup>[19,40,41]</sup>

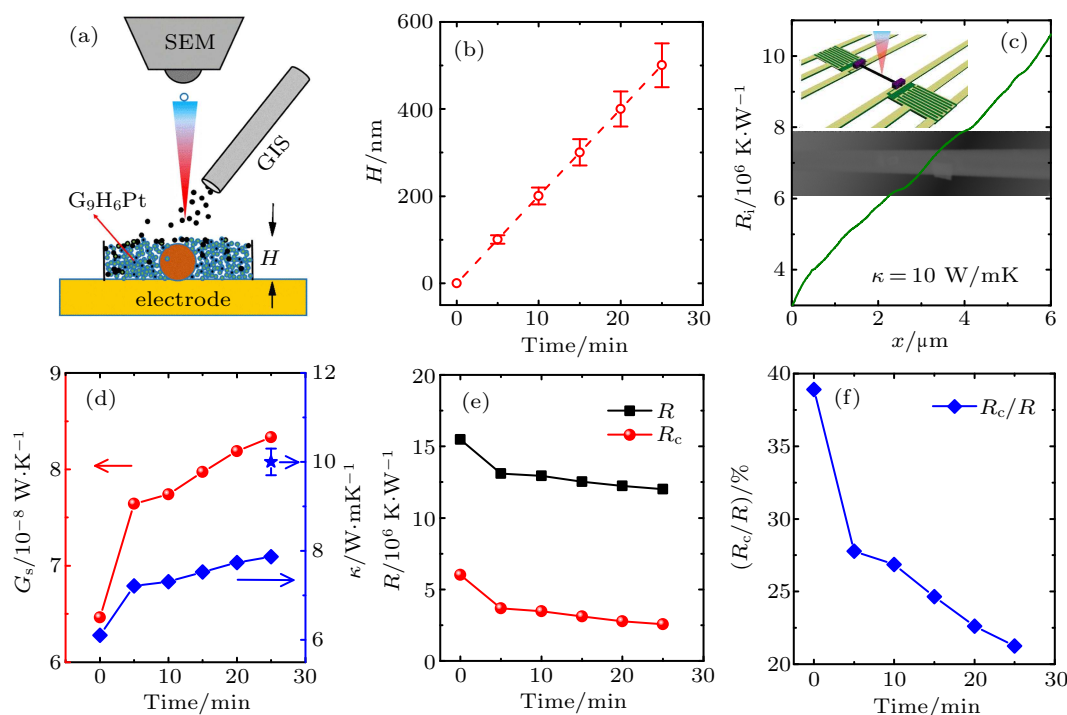


**Fig. 3.** (a) The schematic of the EBID process. (b)  $H$  vs. time shows the Pt/C deposition rate (20 nm/min). The red dash line is the best linear fitting to the data. (c) The typical cumulative thermal resistance ( $R_i$ ) was obtained when the focused electron beam was scanning along the individual nanowires. The upper inset is the schematic of the electron beam self-heating technique and the lower shows the SEM image of the scanned nanowire. (d) Influence of EBID time/height on the thermal contact of the nanowire shown in the lower inset of (c). The red balls and blue diamonds denote the thermal conductance and conductivity measured with the thermal bridge method at  $T = 300$  K for the nanowire, respectively. The blue stars are the intrinsic thermal conductivity derived from the electron beam self-heating technique for the specific nanowire at  $T = 300$  K. (e) The measured thermal resistance  $R$  (black diamonds) and the derived thermal contact resistance  $R_c$  (red balls) of the nanowire vs. time. (f)  $R_c/R$  vs. time. All the solid curves in (d)–(f) are a guide to the eyes.

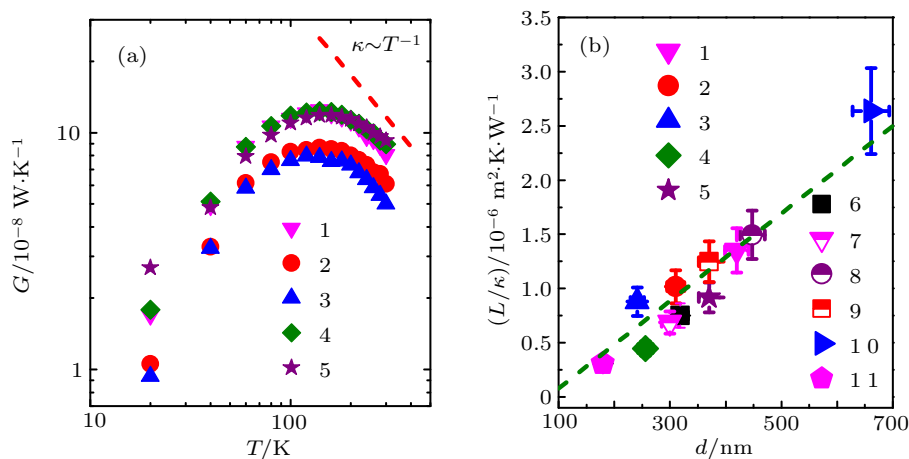


**Fig. 4.** Temperature and size dependent thermal conductivity of the individual nanowires. (a)  $G$  vs.  $T$ . The red dash line shows the  $T^{-1}$  dependency. (b)  $L/\kappa$  vs.  $d$  at  $T = 300$  K, the green dashed line is a guide to the eyes.

As shown in Table 1, the thermal conductivity, measured by the focused electron-beam self-heating method at room temperature, increases with the increasing  $L$ , but decreases with the increasing  $d$ . Distinguished from heat conduction in 3D material,<sup>[42,43]</sup> the thermal conductivities of both 1D and two dimensional materials increase when  $L$  increases. However, it is anomalous for the  $d$  dependent thermal conductivities of the  $\alpha$ -Fe<sub>2</sub>O<sub>3</sub> nanowires as the thermal conductivities of nanowires, like Si nanowires,<sup>[19,40,41]</sup> zinc

oxide nanowires,<sup>[44]</sup> etc., increase with the increasing  $d$  due to surface scatterings and diameter scatterings, except for the graphene<sup>[31,45]</sup> and carbon nanotube<sup>[46,47]</sup> in which the thermal conductivity decreases with increasing thickness/diameter due to suppressing out-of-plane acoustic phonons or due to the smaller phonon hydrodynamics window in thinner graphite flakes.<sup>[48]</sup> Therefore, new theory needs to be proposed to analyze the  $d$  dependent thermal conductivities behavior of the  $\alpha$ -Fe<sub>2</sub>O<sub>3</sub> nanowires.

**Table 1.** Details of the measured individual nanowires.

Samples	1	2	3	4	5	6	7	8	9	10	11
$L/\mu\text{m}$	9.88	6.31	10.47	4.84	5.80	6.63	7.01	16.24	15.78	20.73	11.64
$d/\text{nm}$	420	310	241	256	370	318	300	448	370	661	180
$\kappa/\text{W}\cdot\text{m}^{-1}\cdot\text{K}^{-1}$	7.31	6.21	11.90	10.83	6.31	8.84	10.19	10.86	12.64	7.86	37.72

Here we propose a phenomenological theoretical model to describe the length and diameter dependences of the thermal conductivities of nanowires. For a nanowire, the scattering of phonons usually comes from four parts: boundary scattering, defect/isotopic effect, nonlinear effect, and diameter effect. Here we ignore the defect/isotopic effect since it does not change with the sample size. We also ignore the roughness effect assuming that the surface of the nanowire is smooth enough. The nonlinear effect can be neglected as the phonon mean free path is comparable to the sample length for small nonlinearity close to the ballistic regime. The diameter effect is specific for the nanowires whose diameters are much less than the phonon mean free path. If the diameters are small comparing to the phonon mean free path, the nanowires can be treated as quasi-1D materials. The volume of unit cell will increase as the diameter increases. The larger unit cell will bring more optical phonon branches which will introduce more scattering channels for the acoustic phonons which is responsible for the heat conduction. In another word, the increase of the nanowire diameters will reduce the thermal conductivity if the diameters are much smaller than the phonon mean free path.

Therefore, we can model the phonon scattering rate assuming the Matthiessen's rule as follows:

$$\frac{1}{\tau} = \frac{1}{\tau_{\text{boundary}}} + \frac{1}{\tau_{\text{diameter}}}. \quad (8)$$

The phonon scattering rate can be expressed as  $\tau^{-1} = v/l$ , where  $v$  is the mean phonon velocity and  $l$  is the phonon mean free path. The boundary scattering rate can be simply expressed as  $1/\tau_{\text{boundary}} = v/(\frac{3}{4}L)$ , where  $L$  is the sample length.<sup>[49,50]</sup> And the scattering from diameter effect can be modeled as  $1/\tau_{\text{diameter}} = A(1 - e^{-Bd/l})$ , where  $d$  is the nanowire diameter and  $A$  and  $B$  are two fitting parameters.<sup>[40,51]</sup> For larger enough diameter  $d$ , this term will approach to a saturation value as  $1/\tau_{\text{diameter}} \cong A$ . For small diameter  $d$  compared to the phonon mean free path  $l$ , this term can be approximated as  $1/\tau_{\text{diameter}} \approx A(1 - 1 + Bd/l) = ABd/l$ . It can be seen that the increase of the nanowire diameter will increase the phonon scattering rate and reduce the heat conduction. With all these considerations, the phonon scattering rate can be expressed as

$$\frac{v}{l} = \frac{v}{\frac{3}{4}L} + AB\frac{d}{l}, \quad (9)$$

and we can obtain

$$l = \frac{3}{4}L \left( 1 - \frac{AB}{v}d \right). \quad (10)$$

If we notice that the thermal conductivity  $\kappa$  is proportional to the phonon mean path  $l$ , we can arrive at

$$\kappa \propto L \left( 1 - \frac{AB}{v}d \right), \quad (11)$$

or

$$\frac{\kappa}{L} \propto (1 - Cd), \quad (12)$$

where  $C \equiv AB/v$  is a fitting parameter.  $(1 - Cd) \rightarrow 1/(1 + Cd)$  when  $C \rightarrow 0$ . Hence, we have

$$\kappa \propto \frac{L}{1 + Cd}. \quad (13)$$

Thus, by taking  $L$  and  $d$  into consideration simultaneously,  $\kappa$  could be expressed as a function of the aspect ratio ( $L/(1 + Cd)$ ), where  $C$  is a constant, i.e.,  $\kappa$  increases with the aspect ratio increasing. Here, it is worthy to note that the thermal conductivities of individual  $\alpha\text{-Fe}_2\text{O}_3$  nanowires are not only  $L$  but  $d$  dependent simultaneously. To analyze the size dependence of  $\kappa$  clearly, equation (13) can be transferred into  $L/\kappa \propto d$ . The experimental results of Table 1 are shown in Fig. 4(b). Figure 4(b) indicates that  $L/\kappa$  is linear with  $d$ .  $L/\kappa$  increases from  $\sim 3.1 \times 10^{-7} \text{ m}^2 \cdot \text{K} \cdot \text{W}^{-1}$  to  $\sim 2.6 \times 10^{-6} \text{ m}^2 \cdot \text{K} \cdot \text{W}^{-1}$  as  $d$  increases from 180 nm to 661 nm. This shows that the anomalous thermal conductivities are consistent with the theory and the thermal conductivities of the measured samples can be expressed as  $\kappa \propto L/(1 + Cd)$ .

## 4. Conclusion

We measured the thermal conductivity of individual single crystalline  $\alpha\text{-Fe}_2\text{O}_3$  nanowires with thermal bridge method and focused electron-beam self-heating technique based on prepatterned suspended device in the temperature range from 20 K to 300 K. EBID process obviously improved the contact condition and the thermal contact resistances were reduced to about 20% or less of the total thermal resistance. Thermal conductivity was not only  $L$  but  $d$  dependent simultaneously and diverged anomalously with the aspect ratio as  $\kappa \propto L/(1 + Cd)$  in the measured samples with diameter ( $d$ ) ranging from 180 nm to 661 nm and length ( $L$ ) changing from 4.84  $\mu\text{m}$  to 20.73  $\mu\text{m}$ . Rigorous calculations and more experiments are needed to further prove whether this divergence is universal in  $\alpha\text{-Fe}_2\text{O}_3$  nanowires.

## References

- [1] Bertelsen P, Goetz W, Madsen M B, Kinch K M, Hviid S F, Knudsen J M, Gunnlaugsson H P, Merrison J, Nornberg P, Squyres S W, Bell J F, 3rd, Herkenhoff K E, Gorevan S, Yen A S, Myrick T, Klingelhofer G, Rieder R and Gellert R 2004 *Science* **305** 827
- [2] Jubb A M and Allen H C 2010 *Acs Appl. Mater. Inter.* **2** 2804
- [3] Weiss W, Zscherpel D and Schlogl R 1998 *Catal. Lett.* **52** 215
- [4] Faust B C, Hoffmann M R and Bahnmann D W 1989 *J. Phys. Chem.* **93** 6371
- [5] Ohmori T, Takahashi H, Mametsuka H and Suzuki E 2000 *Phys. Chem. Chem. Phys.* **2** 3519
- [6] Comini E, Faglia G and Sberveglieri G 2001 *Sensor. Actuat. B-Chem.* **78** 73
- [7] Comini E, Guidi V, Frigeri C, Ricco I and Sberveglieri G 2001 *Sensor. Actuat. B-Chem.* **77** 16
- [8] Gupta A K and Gupta M 2005 *Biomaterials* **26** 3995
- [9] del Pino P, Munoz-Javier A, Vlaskou D, Rivera Gil P, Plank C and Parak W J 2010 *Nano Lett.* **10** 3914
- [10] Nakamura T 1977 *Sol. Energy* **19** 467
- [11] Poizot P, Laruelle S, Grugeon S, Dupont L and Tarascon J M 2000 *Nature* **407** 496
- [12] Wan X, Feng W, Wang Y, Wang H, Zhang X, Deng C and Yang N 2019 *Nano Lett.* **19** 3387
- [13] Collins P G, Bradley K, Ishigami M and Zettl A 2000 *Science* **287** 1801
- [14] Cui Y and Lieber C M 2001 *Science* **291** 851
- [15] Hong S and Myung S 2007 *Nat. Nanotechnol.* **2** 207
- [16] Chang C W, Okawa D, Majumdar A and Zettl A 2006 *Science* **314** 1121
- [17] Xie R G, Bui C T, Varghese B, Zhang Q X, Sow C H, Li B W and Thong J T L 2011 *Adv. Funct. Mater.* **21** 1602
- [18] Chan C K, Peng H, Liu G, McIlwrath K, Zhang X F, Huggins R A and Cui Y 2008 *Nat. Nanotechnol.* **3** 31
- [19] Yang N, Zhang G and Li B W 2010 *Nano Today* **5** 85
- [20] Tian B Z, Zheng X L, Kempa T J, Fang Y, Yu N F, Yu G H, Huang J L and Lieber C M 2007 *Nature* **449** 885
- [21] Boukai A I, Bunimovich Y, Tahir-Kheli J, Yu J K, Goddard W A 3rd and Heath J R 2008 *Nature* **451** 168
- [22] Wen X, Wang S, Ding Y, Wang Z L and Yang S 2005 *J. Phys. Chem. B* **109** 215
- [23] Lee Y C, Chueh Y L, Hsieh C H, Chang M T, Chou L J, Wang Z L, Lan Y W, Chen C D, Kurata H and Isoda S 2007 *Small* **3** 1356
- [24] Lin Y, Sun F Q, Yuan X Y, Geng B Y and Zhang L D 2004 *App. Phys. A* **78** 1197
- [25] Wu J J, Lee Y L, Chiang H H and Wong D K 2006 *J. Phys. Chem. B* **110** 18108
- [26] Liu L, Kou H Z, Mo W, Liu H and Wang Y 2006 *J. Phys. Chem. B* **110** 15218
- [27] Tang B, Wang G, Zhuo L, Ge J and Cui L 2006 *Inorg. Chem.* **45** 5196
- [28] Dong L, Xi Q, Zhou J, Xu X and Li B 2020 *Phys. Rev. Appl.* **13** 034019
- [29] Dong L, Xi Q, Chen D, Guo J, Nakayama T, Li Y, Liang Z, Zhou J, Xu X and Li B 2018 *Natl. Sci. Rev.* **5** 500
- [30] Shi L, Li D, Yu C, Jang W, Kim D, Yao Z, Kim P and Majumdar A 2003 *J. Heat Trans.* **125** 881
- [31] Xu X, Pereira L F, Wang Y, Wu J, Zhang K, Zhao X, Bae S, Tinh Bui C, Xie R, Thong J T, Hong B H, Loh K P, Donadio D, Li B and Ozyilmaz B 2014 *Nat. Commun.* **5** 3689
- [32] Kim P, Shi L, Majumdar A and McEuen P L 2001 *Phys. Rev. Lett.* **87** 215502
- [33] Guo J, Huang Y, Wu X, Wang Q, Zhou X, Xu X and Li B 2019 *Phys. Status Solidi-RRL* **13** 1800529
- [34] Wang Q, Liang X, Liu B, Song Y, Gao G and Xu X 2020 *Nanoscale* **12** 1138
- [35] Aiyiti A, Hu S, Wang C, Xi Q, Cheng Z, Xia M, Ma Y, Wu J, Guo J, Wang Q, Zhou J, Chen J, Xu X and Li B 2018 *Nanoscale* **10** 2727
- [36] Liu D, Xie R, Yang N, Li B and Thong J T 2014 *Nano Lett.* **14** 806
- [37] Zhao Y, Liu D, Chen J, Zhu L, Belianinov A, Ovchinnikova O S, Unocic R R, Burch M J, Kim S, Hao H, Pickard D S, Li B and Thong J T L 2017 *Nat. Commun.* **8** 15919
- [38] Aiyiti A, Bai X, Wu J, Xu X and Li B 2018 *Sci. Bull.* **63** 452
- [39] Khitun A, Balandin A and Wang K L 1999 *Superlattice. Microst.* **26** 181
- [40] Li D Y, Wu Y Y, Kim P, Shi L, Yang P D and Majumdar A 2003 *Appl. Phys. Lett.* **83** 2934
- [41] Chen R, Hochbaum A I, Murphy P, Moore J, Yang P and Majumdar A 2008 *Phys. Rev. Lett.* **101** 105501
- [42] Saito K and Dhar A 2010 *Phys. Rev. Lett.* **104** 040601
- [43] Wang L, He D and Hu B 2010 *Phys. Rev. Lett.* **105** 160601
- [44] Yuldashev Sh U, Yalishev V, Cho H D and Kang T W 2016 *J. Nanosci. Nanotechnol.* **16** 1592
- [45] An M, Song Q, Yu X, Meng H, Ma D, Li R, Jin Z, Huang B and Yang N 2017 *Nano Lett.* **17** 5805
- [46] Lee V, Wu C H, Lou Z X, Lee W L and Chang C W 2017 *Phys. Rev. Lett.* **118** 135901
- [47] Yue S Y, Ouyang T and Hu M 2015 *Sci. Rep.* **5** 15440
- [48] Machida Y, Matsumoto N, Isono T, Behnia K 2020 *Science* **367** 309
- [49] Majumdar A 1993 *J. Heat Trans.* **115** 7
- [50] Hao Q, Xiao Y and Chen Q 2019 *Mater. Today Phys.* **10** 100126
- [51] Morse P M 1929 *Phys. Rev.* **34** 57